Chemical bonding in initial building blocks of semiconductors

Jäger, Marc; Shayeghi, Armin; Klippenstein, Viktor; Johnston, Roy; Schäfer, Rolf

DOI:
10.1063/1.5066414

Chemical bonding in initial building blocks of semiconductors: Geometrical structures and optical absorption spectra of isolated $CdSe_2^+$ and $Cd_2Se_2^+$ species

Marc Jäger, Armin Shayeghi, Viktor Klippenstein, Roy L. Johnston, and Rolf Schäfer

Citation: J. Chem. Phys. **149**, 244308 (2018); doi: 10.1063/1.5066414
View online: https://doi.org/10.1063/1.5066414
View Table of Contents: http://aip.scitation.org/toc/jcp/149/24
Published by the American Institute of Physics

Chemical bonding in initial building blocks of semiconductors: Geometrical structures and optical absorption spectra of isolated $CdSe_2^+$ and $Cd_2Se_2^+$ species

Marc Jäger,[1,a)] Armin Shayeghi,[1,2] Viktor Klippenstein,[1] Roy L. Johnston,[3] and Rolf Schäfer[1]

[1]*Technische Universität Darmstadt, Eduard-Zintl-Institut, Alarich-Weiss-Straße 8, 64287 Darmstadt, Germany*

[2]*Vienna Center for Quantum Science and Technology, Faculty of Physics, University of Vienna, Boltzmanngasse 5, A-1090 Vienna, Austria*

[3]*School of Chemistry, University of Birmingham, Edgbaston, Birmingham B15 2TT, United Kingdom*

(Received 15 October 2018; accepted 4 December 2018; published online 28 December 2018)

We present the first experimental optical absorption spectra of isolated $CdSe_2^+$ and $Cd_2Se_2^+$ species in the photon energy range $\hbar\omega$ = 1.9–4.9 eV. We probe the optical response by measuring photodissociation cross sections and combine our results with time-dependent density functional theory and equation-of-motion coupled cluster calculations. Structural candidates for the time-dependent excited state calculations are generated by a density functional theory based genetic algorithm as a global geometry optimization tool. This approach allows us to determine the cluster geometries present in our molecular beams by a comparison of experimental spectra with theoretical predictions for putative global minimum candidates. For $CdSe_2^+$, an excellent agreement between the global minimum and the experimental results is presented. We identify the global minimum geometry of $Cd_2Se_2^+$ as a trapezium, which is built up of a neutral Se_2 and a cationic Cd_2^+ unit, in contrast to what was previously proposed. We find an excellent overall agreement between experimental spectra and excited state calculations. We further study the influence of total and partial charges on the optical and geometric properties of Cd_2Se_2 and compare our findings to CdSe quantum dots and to bulk CdSe. *Published by AIP Publishing.* https://doi.org/10.1063/1.5066414

I. INTRODUCTION

The rising trend towards more digitalization in almost all areas of daily life has led to an increased demand for smaller, faster, and more powerful electronic devices.[1–6] This has accelerated the investigation of nanoscale and subnanoscale semiconductor materials. In particular, the exploration of small II-VI semiconductor nanoparticles (NPs) such as CdSe quantum dots (QDs) has drawn significant attention due to their intriguing optoelectronic properties, which makes them promising materials for optical applications such as displays, solar cells, lasers, light emitting diodes (LEDs), and biomedical imaging.[7–13] One major goal in nanoscience is to tailor such materials at the atomic scale and to tune material properties very precisely for future technologies. To achieve this, a fundamental understanding of the size-dependent development of the properties of interest is absolutely necessary. While much is known about II-VI semiconductor systems (e.g., CdSe) in the bulk phase[14–16] as well as for larger CdSe NPs,[17–38] less information is available about their behavior at very small sizes in the form of clusters consisting of only a few atoms.

Many reported experimental studies are focused on the synthesis and characterisation of optical properties of colloidal, stoichiometric, and neutral CdSe clusters.[24–38] It has been observed that with smaller particle size, the optical emission and absorption become blue-shifted due to quantum confinement effects.[13,32,39–47] Hence, the photoluminesence of small semiconductor NPs can be tuned by varying the cluster size. Besides the dimensions, the optical properties of these clusters are also highly dependent on other parameters such as composition, temperature, charge, or chemical environment.[26,29,31,37]

In contrast to the previously mentioned investigations of colloidal (ligated) CdSe systems, significantly less information is available about naked CdSe clusters. Orii *et al.* measured photoluminescence spectra for isolated CdSe clusters in the size range 6–26 nm, without specifying the exact number of atoms in each cluster.[48] They recorded the cumulated optical properties for all particles in a molecular beam of CdSe in the energy range $\hbar\omega$ = 1.5–2.5 eV. Zang *et al.* generated CdSe nanoparticles in the gas phase with a magnetron sputter source in order to prepare deposited nanoparticles.[49] The mean diameter of their clusters was approximately 4.8 nm, with a resulting bandgap energy of about 2.8 eV, which is significantly blue-shifted compared to the bulk value of 1.7 eV (due to the previously mentioned quantum confinement effect). Very stable CdSe clusters were synthesized in toluene solution by

a)Author to whom correspondence should be addressed: jaeger@cluster.pc.chemie.tu-darmstadt.de

Kasuya *et al.* and investigated in the gas phase by time-of-flight mass spectrometry (TOF-MS).[50] The mass spectra revealed the existence of very stable $Cd_{33}Se_{33}$ and $Cd_{34}Se_{34}$ species. Optical absorption spectra of the corresponding CdSe cluster solutions were also recorded and show a sharp excitonic peak at 2.99 eV (with smaller peaks at 3.25 eV and 3.52 eV). Density functional theory (DFT) calculations predict that $Cd_{33}Se_{33}$ and $Cd_{34}Se_{34}$ are built up of puckered $Cd_{28}Se_{28}$ cages (highly symmetric analogs of fullerenes) with a Cd_5Se_5 or Cd_6Se_6 core structure, respectively.

Stoichiometric neutral $(CdSe)_n$ clusters have been extensively investigated computationally. The geometries, electronic structures, and optical properties of neutral Cd_nSe_n clusters up to $n = 60$ (the particle diameter size is approximately 1.7 nm for $n = 60$) were studied by DFT and time-dependent density functional theory (TDDFT) calculations.[51–60] All cluster geometries were found to exhibit alternating Cd-Se bonds and mainly obey Euler's theorem (for convex polyhedra).[61] Cd_nSe_n clusters with $n \geq 8$ are built up from alternating four-membered and six-membered rings. Ring-like structures with heteronuclear bonds have been found to be the lowest lying structures up to $n = 4$, and spheroid structures have been predicted for larger particles.

To the best of our knowledge, there has only been one experimental study of small bare cationic CdSe clusters.[62] Only mass spectra of small cationic CdSe clusters were recorded, without measuring any further physical or chemical properties. This was also the first theoretical study of positively charged stoichiometric CdSe cluster structures. For stoichiometric $Cd_nSe_n^+$ ($1 \leq n \leq 16$), cluster geometries and incremental atomisation energies were computed at the B3LYP/SKBJ level of theory. For small clusters up to $n = 5$, the same global minimum (GM) cluster structures were found as for the neutral counterparts.

The scientific objective of gaining a fundamental understanding of the intrinsic optoelectronic properties of CdSe clusters can be achieved with a combined experimental and theoretical bottom-up approach, by starting with very small and isolated species and gradually increasing the complexity (such as system size, composition, and chemical environment). Here, we present the first optical absorption spectra of bare $CdSe_2^+$ and $Cd_2Se_2^+$ cations in the photon energy range $\hbar\omega$ = 1.9–4.9 eV, recorded by longitudinal photodissociation spectroscopy.[63] These photodissociation spectra are also the first that have been measured utilising the sum frequency mixing (SFM) extension of our tunable laser system. We support our experimental results with optical response calculations using TDDFT and equation-of-motion coupled cluster singles and doubles (EOM-CCSD) methods. Energetically low-lying isomers are obtained by an unbiased global optimisation procedure using a genetic algorithm (GA) at the DFT level of theory. Furthermore, we investigate the influence of the charge on the structural and optical properties of $Cd_2Se_2^q$ ($q = -1$, 0, +1). Additionally, in the supplementary material, we provide a benchmark of different basis sets and exchange correlation (xc) functionals for the calculations of the optical properties of $Cd_nSe_m^+$, making a direct comparison with the experimental data. Our findings may serve as the basis for the study of larger CdSe clusters.

II. EXPERIMENTAL AND COMPUTATIONAL DETAILS

A. Experimental details

The general methodology and experimental details are described elsewhere;[63] therefore, only a brief overview is given here. The experimental setup is shown in Fig. 1. Cadmium-selenide cluster cations are generated in a laser vaporisation source by focusing the second harmonic generation (SHG) of a Nd:YAG laser onto a rotating and translating CdSe target (American Elements, composition: Cd:Se = 50:50, purity: 99.999%) in a He buffer gas environment. The generated clusters are detected by time-of-flight mass spectrometry (TOF-MS). Optical absorption spectra are recorded by longitudinal photodissociation spectroscopy employing an optical parametric oscillator (OPO), which covers the photon energy range $\hbar\omega$ = 1.9–4.9 eV. By using the recently installed SFM setup in the UV range (the SFM is available in the range 3.04–4.19 eV),

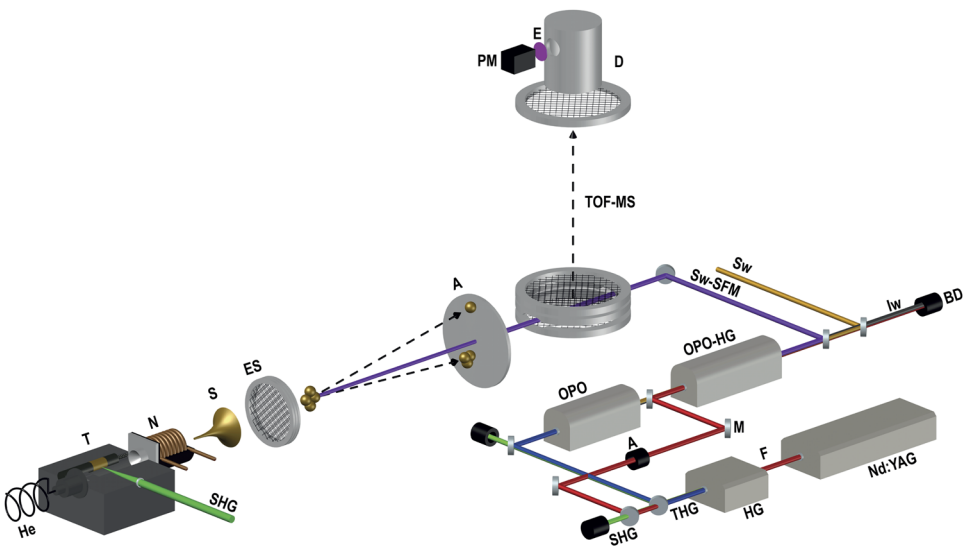

FIG. 1. Scheme of the experimental setup with SFM extension for the tunable laser system (He: Helium valve, SHG: Second harmonic generation of a Nd:YAG laser, T: Translating and rotating CdSe target, N: Nozzle, S: Skimmer, ES: Electrostatic shutter, A: Aperture, TOF-MS: Time of flight mass spectrometer, D: Detector system, E: Electron scintillator, PM: Photomultiplier, Nd:YAG: Nd:YAG pump laser, F: Fundamental of a Nd:YAG laser, HG: Harmonic Generator, THG: Third harmonic generation of a Nd:YAG laser, M: Mirror, OPO: Optical parametric oscillator, OPO-HG: Harmonic generator, BD: Beam dump, Sw: Signal wave, Iw: Idler wave, SW-SFM: Sum frequency mixing signal wave).

a highly increased photon fluence and much improved laser pulse stability were obtained. This is achieved by mixing the fundamental (F, 1064 nm) of the Nd:YAG laser with the OPO signal wave (Sw) output in the second SHG/SFM stage (OPO-HG). The improvement of the new laser setup is demonstrated in Table I, which compares the lowest and highest laser fluence for the old (SHG) and new (SFM) laser systems. In addition, we have extended the range of our tunable dissociation laser by 0.5 eV, and hence, a maximum energy of 4.9 eV is accessible. For the whole UV-VIS spectral range, only the more powerful signal wave (Sw) was used, whereas the idler wave (Iw) was guided into a beam dump (BD). The TOF-MS operates at 10 Hz, while the tunable laser system is triggered by 5 Hz, which allows a simultaneous storage of mass spectra with and without the laser radiation per wavelength. Finally, the experimental absorption spectra [the absorption cross section $\sigma(\hbar\omega)$ as a function of the photon energy] are obtained by applying the Lambert-Beer law[63] for one-photon absorption processes and assuming a perfect overlap between the molecular beam and the dissociation laser, as in earlier studies.[64–67] Consequently, the photodissociation cross sections presented should be considered as lower limits to the total absorption cross sections.

B. Computational details

In the present study, we perform a global optimization of the configurational space of $CdSe_2^+$ and $Cd_2Se_2^+$, using the Mexican enhanced genetic algorithm (MEGA),[68] an improved version of the Birmingham parallel genetic algorithm (BPGA),[69,70] to create suitable structural candidates. This is done at the plane-wave density functional level of theory (pw-DFT). Local geometry optimizations use the Vienna *ab initio* Simulation Package (VASP) code[71–74] with the Perdew-Burke-Ernzerhof (PBE) exchange-correlation (xc) functional and projected augmented wave (PAW) pseudopotentials.[75,76] The plane-wave basis set was truncated with a cut-off energy at 400 eV, and spin polarisation was implemented.

All lowest lying isomers are locally reoptimized using NWChem v.6.6[77] (orbital-based DFT, using tight optimization criteria and a high density numerical grid), employing the hybrid xc functionals PBE0[78] and B3LYP[79] and the correlation-consistent cc-pVTZ-PP basis set. For Cd and Se, 20 and 24 electrons are treated explicitly, respectively.[80–82] The choice of functionals and basis sets is justified by our benchmark calculations (see the supplementary material). Furthermore, for geometry refinement, we also employed the more demanding coupled clusters singles and doubles (CCSD) approach as well as coupled cluster singles doubles with perturbative triples CCSD(T). Hence, we reoptimize all lowest energy structures at the CCSD/cc-pVTZ-PP level of theory and evaluate the resulting isomer structures with single point energy calculations at the CCSD(T)/cc-pVTZ-PP level of theory using Gaussian09.[83] Harmonic frequency analyses are performed for all isomers at the particular level of theory, in order to verify that the optimized geometries correspond to local minima on the potential energy surface. For geometries generated in this way, electronic excitation spectra are calculated using spin-unrestricted TDDFT, with 60 excited states, employing the same xc functionals and basis sets as used in the geometry optimizations. In Gaussian09,[83] EOM-CCSD optical response calculations with 40 excited states are also performed for all geometries obtained by CCSD. For all structures, a natural bond analysis (NBA) is conducted at the PBE0/cc-pVTZ-PP level of theory. Previously we have successfully demonstrated the capability of this combined experimental and theoretical approach for the structure discrimination of small Ag, Au, and AgAu clusters.[63–67]

TABLE I. Effect of the SFM enhancement with respect to the photon fluence Φ. The maximum and minimum photon fluence Φ_{max} and Φ_{min} are shown for the energy range 3.04–4.19 eV for both the old SHG and the new SFM setup.

	$\Phi_{min}/Å^{-2}$		$\Phi_{max}/Å^{-2}$	
Energy range/eV	SHG	SFM	SHG	SFM
3.04–4.19	0.05	0.95	0.59	1.88

III. RESULTS AND DISCUSSION

A. $CdSe_2^+$ cluster structures

In the case of $CdSe_2^+$, no further isomer was found within 0.50 eV of the putative global minimum at all considered levels of theory. The next higher lying isomer is separated by approximately 1.50 eV. Both structures are depicted in Fig. 2, and the bond lengths are presented in Table II. The putative GM (Iso-I) is a C_s (bent Cd–Se–Se) structure with a singly coordinated Cd. The next isomer, with linear (Se–Cd–Se) geometry and $C_{\infty v}$ symmetry (Iso-II), lies much higher in energy [1.48 eV for CCSD(T)]. In contrast to neutral stoichiometric $(CdSe)_n$ clusters, the most stable isomer (Iso-I) does not have alternating Cd–Se bonds; instead, a Se–Se unit is the fundamental building block. It is noticeable that the relative DFT energies computed with the PBE0 functional are closer to the CCSD(T) values than those obtained by B3LYP calculations. For both structures, the positive charge is mainly localized on the Cd atom as shown by the natural bond analysis. For Iso-I, this effect is more marked. For Iso-II, the natural charges are

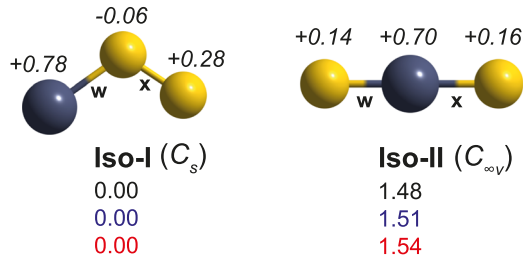

FIG. 2. Lowest lying $CdSe_2^+$ isomers (Cd: dark atoms, Se: light atoms) and their relative energies in eV, as obtained at the CCSD(T)/cc-pVTZ (black), PBE0/cc-pVTZ-PP (blue), and B3LYP/cc-pVTZ-PP (red) levels of theory together with their point group symmetries. Natural charges from NBA are given in italic font. The chemical bonds are labeled with w and x.

TABLE II. Bond lengths (in Å) for bonds w and x shown in Fig. 2 at the PBE0/cc-pVTZ-PP level of theory.

Bond	Iso-I	Iso-II
w	2.69	2.44
x	2.17	2.52

different on the two Se atoms, which reflects the slightly different Cd–Se bond lengths (cf. Table II). The Cd–Se bond of Iso-I is significantly larger than the Cd–Se bonds of Iso-II. Consistent with this, the NBA shows that Iso-I can be considered as a Cd^+ cation bonded to a neutral Se_2 dimer.

B. $Cd_2Se_2^+$ cluster structures

The lowest lying isomers for $Cd_2Se_2^+$ are presented in Fig. 3. Additionally the bond lengths are shown in Table III. We found four different structural candidates within 0.50 eV. All isomers are planar. The putative GM (Iso-I) is a distorted trapezium with C_{2v} symmetry and can be considered as two parallel aligned dimers (Se_2 and Cd_2) bonded to each other. Iso-II exhibits a "Y"-shape (with C_{2v} symmetry) and can also be regarded as built up from Se_2 and Cd_2 dimers, but with orthogonal alignment and an inner three-fold coordinated Cd atom. Iso-III, with C_s symmetry, displays a distorted "L"-shape. Again, it is formed of linked Se_2 and Cd_2 dimers. Iso-III appears to be a true minimum only at the DFT level because after geometry optimization at the CCSD level, Iso-III relaxed to Iso-II. Therefore, we used the PBE0/cc-pVTZ-PP geometry as input for the single point CCSD(T)/cc-pVTZ-PP

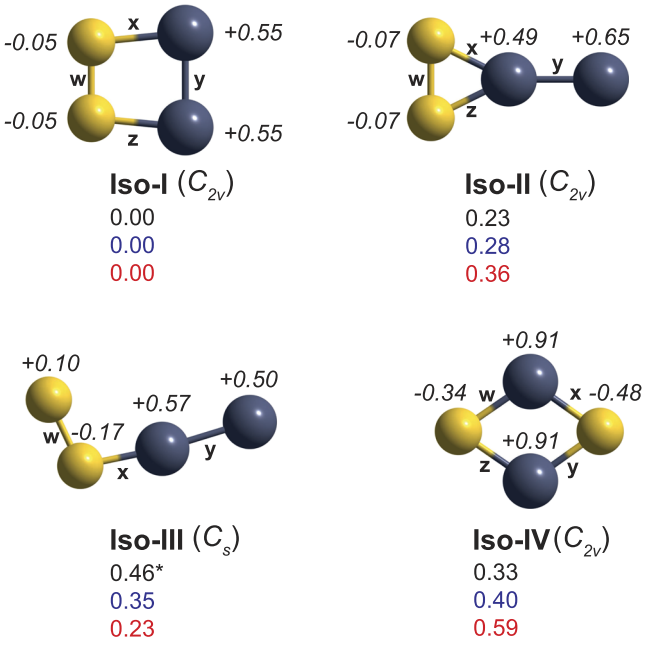

FIG. 3. Lowest lying $Cd_2Se_2^+$ isomers (Cd: dark atoms, Se: light atoms) and their relative energies in eV, as obtained at the CCSD(T)/cc-pVTZ (black), PBE0/cc-pVTZ-PP (blue), and B3LYP/cc-pVTZ-PP (red) levels of theory together with their point group symmetries. The star * indicates the CCSD(T) energy calculation for the geometry relaxed at the PBE0/cc-pVTZ-PP level of theory. Natural charges from NBA are given in italic font. The chemical bonds are labeled with w, x, y, and z.

TABLE III. Bond lengths (in Å) for bonds w, x, y, and z shown in Fig. 3 at the PBE0/cc-pVTZ-PP level of theory.

Bond	Iso1-I	Iso-II	Iso-III	Iso-IV
w	2.21	2.33	2.21	2.59
x	2.76	2.57	2.55	2.53
y	2.75	2.70	2.79	2.53
z	2.76	2.57		2.59

calculation. Only Iso-IV, a slightly distorted rhombus with C_{2v} symmetry, shows completely alternating Cd and Se atoms, but with different Cd–Se bond lengths (cf. Table III). Regarding the relative energies, Iso-I is always the putative GM and is geometrically related to Iso-I of $CdSe_2^+$ by adding a Cd atom, so as to form one Cd–Cd bond and another Cd–Se bond. As in the case of $CdSe_2^+$, the relative energies obtained with PBE0 are closer to the CCSD(T) results than the B3LYP energies. For all structures, the positive charge is mainly localized on the Cd-atoms, but for Iso-I, the NBA shows two distinct units, the almost neutral Se_2 and charged Cd_2^+. Consistent with this, Iso-I shows the largest Se–Cd bond-length. The formation of a covalent Se_2 bond has also been reported for the dicationic $Cd_2Se_2^{2+}$ species.[84]

For $Cd_2Se_2^+$, a clear stability trend is observed. Isomers composed of Se_2 and Cd_2 dimers are energetically preferred, in contrast to Iso-IV [with the exception of Iso-III at CCSD(T)]. This is surprising because the GMs of neutral stoichiometric $(CdSe)_n$ clusters form structures, with alternating Cd and Se atoms (as in Iso-IV).[53–55,59] Sanville *et al.*[62] proposed Iso-IV as the GM structure for both the neutral and cationic species at the less precise B3LYP/SKBJ level of theory, but with the constraint that only structures with heteronuclear bonding were considered. With this restriction, it was not possible to find the structures of Iso-I to Iso-III, which highlights the importance of an unbiased global optimization of a cluster system of interest, to actually find the GM structure.

C. Influence of charge q (= −1, 0, +1) on the structure of $Cd_2Se_2^q$ clusters

In order to further investigate the influence of charge on the structural motifs of Iso-I and Iso-IV, the calculated energies for both isomers at different levels of theory for several charge states are listed in Table IV. Additionally, Mulliken charges and natural charges (cf. Fig. 4), bond lengths (cf. Table V), highest occupied molecular orbitals (HOMOs) and lowest unoccupied molecular orbitals (LUMOs), and atomic orbital projected density of states (pDOS) (cf. Fig. 5) have been calculated. We performed the calculations for the Mulliken charges and pDOS with NWChem at the PBE0/cc-pVTZ-PP level of theory. According to Table IV, for larger basis sets, cationic Iso-I is always lower in energy than Iso-IV, while the opposite is found for the neutral and anionic species. Iso-IV is only preferred for the positively charged species for small basis sets (PBE0/sbkjc-vdz and PBE0/lanl2dz), while in the case of B3LYP/lanl2dz, the energy separation of these isomers seems to be strongly underestimated. Hence, a small

TABLE IV. Influence of the quantum chemical method, basis set, and charge q on the relative energies of Iso-I and Iso-IV of $Cd_2Se_2^q$ for the cationic ($q = +1$), the neutral ($q = 0$), and anionic ($q = -1$) species. Relative energies after geometry refinement are presented.

	ΔE/eV = (E(Iso-IV) − E(Iso-I))/eV		
Method/basis set	Cation	Neutral	Anion
CCSD(T)/cc-pVTZ-PP	0.33	−0.71	−0.87
CCSD/cc-pVTZ-PP	0.20	−0.81	−0.84
PBE0/cc-pVTZ-PP	0.40	−0.68	−0.77
B3LYP/cc-pVTZ-PP	0.59	−0.43	−0.51
PBE0/def2-tzvpp	0.39	−0.69	−0.77
HSE06/def2-tzvpp	0.42	−0.64	−0.72
PBE0/sbkjc-vdz	−0.28	−1.12	−1.12
B3LYP/sbkjc-vdz	0.01	−0.79	−0.78
PBE0/lanl2dz	−0.39	−1.20	−1.12

basis set seems to be insufficient for the energetic description of $Cd_2Se_2^+$, especially by direct comparison with the CCSD(T)/cc-pVTZ-PP values. In general, it can be seen that Iso-IV is increasingly favored as the number of valence electrons increases from the cation, to neutral to anion, and thus by varying the charge, the GM structure motif changes. An unbiased global optimization of neutral ($q = 0$) and anionic ($q = -1$) $Cd_2Se_2^q$ using MEGA reveals that Iso-IV is the GM for both charge states. Irrespective of the charge, the values calculated with PBE0/cc-pVTZ-PP are closer to the CCSD(T)/cc-pVTZ-PP results than the B3LYP/cc-pVTZ-PP energy differences. The analysis of bond length with respect to the charge (cf. Table V and Figs. 3 and 4 of the supplementary material) shows that in the case of Iso-I, the homonuclear bonds (Cd–Cd and Se–Se) increase with the number of electrons, while the heteronuclear Cd–Se bond lengths show a minimum for the neutral species for both isomers Iso-I and Iso-IV. The Cd–Se bond lengths are shorter in Iso-IV than in Iso-I for all charges q.

Figure 4 shows the results of the NBA and the Mulliken population analysis for cationic, neutral, and anionic Iso-I and Iso-IV. Taking into account that Mulliken population analysis strongly depends on the quantum chemical method and basis set size, here it can still be used to qualitatively describe the charge dependence because the Mulliken charges show the same trend as the natural charges. For cationic Iso-I, the positive charge is almost entirely localized on the more electropositive Cd atoms. Hence, Iso-I can be considered as a neutral Se_2 unit bonded in parallel to a cationic Cd_2^+ dimer. The influence of the charges on the geometry of Iso-IV can be clearly recognized by considering the natural and Mulliken charges. The neutral and anionic species exhibit D_{2h} symmetry with equal bond distances and identical charges for both Se atoms (negative) and both Cd atoms (positive). The positive charge lowers the symmetry of Iso-IV to C_{2v} with slightly different bond distances (cf. Table V and Figs. 3 and 4 of the supplementary material), and also the charges on the Se atoms differ. Independent of the charge state, the chemical bonds in Iso-IV exhibit much greater ionic character than those in Iso-I. Hence Iso-IV is more similar to fragments of bulk CdSe than Iso-I in terms of the polarity of the bonds. The partial charges for all species behave according to their electronegativities (EN): EN(Se) > EN(Cd). Consequently, Se always exhibits a more negative partial charge than Cd.

The pDOS for cationic Iso-I and Iso-IV, shown in Fig. 5, is obtained by projection of the molecular orbitals on the atomic basis set. The pDOS was calculated with spin unrestricted DFT (PBE0/cc-pVTZ-PP, doublet spin multiplicity), which results in a separate α-pDOS and β-pDOS for electrons with "spin-up" and "spin-down," respectively. The HOMOs and LUMOs and the HOMO-LUMO gaps (ΔE_{HL}) are also shown in Fig. 5. The visualisation of the orbitals and the MO analysis was carried out using Chemissian.[85] The larger ΔE_{HL} for Iso-I indicates a higher kinetic stability.[51] Since in bulk CdSe the conduction band mainly consists of s orbitals on Cd atoms, while the valance band is composed of p orbitals from Se,[44,86] Se-p and Cd-s basis function contributions to the total pDOS are shaded in yellow and orange, respectively, in Fig. 5. Regarding the β-orbitals of Iso-IV, there is a very small HOMO-LUMO gap $\Delta E_{\beta-HL}$ = 1.62 eV from a bonding HOMO to an antibonding LUMO. Comparison of the HOMOs of Se_2 and Iso-I reveals a high similarity, which supports the idea that Iso-I consists of a neutral Se_2 and a cationic Cd_2^+ unit. Hence, the HOMO of Iso-I is mainly localized on the two Se atoms and is formed from Se-p orbitals. The HOMOs and the nearby bonding-states (i.e., lower energy states) of both isomers are significantly dominated by Se-p basis functions, whereas the LUMO also has a significant contribution of Cd-s basis functions, though the β-LUMO is also dominated by Se-p functions for both isomers. The α-HOMO and α-LUMO compositions are similar to the previously mentioned compositions of the valence and conduction bands of bulk CdSe.[44,86] The same dominant basis function contributions to the HOMO and LUMO

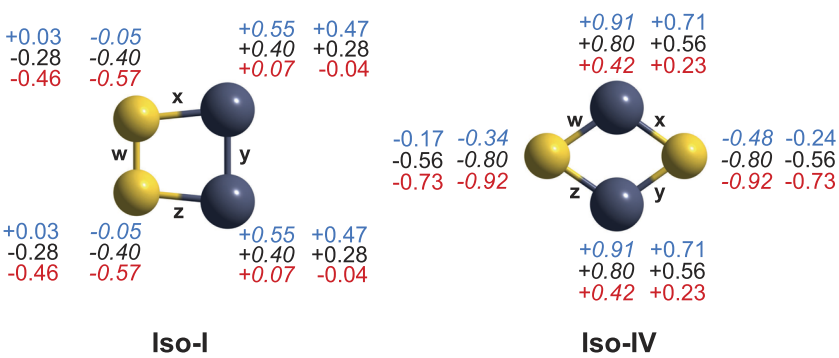

FIG. 4. Natural (italic font) and Mulliken (normal font) charges for Iso-I and Iso-IV (Cd: dark atoms, Se: light atoms) for cationic (blue), neutral (black), and anionic (red) species are calculated at the PBE0/cc-pVTZ-PP level of theory.

TABLE V. Bond lengths (in Å) for bonds w, x, y, and z shown in Fig. 4 at the PBE0/cc-pVTZ-PP level of theory for different charge states of Iso-I and Iso-IV.

	Iso-I			Iso-IV		
Bond	Cation	Neutral	Anion	Cation	Neutral	Anion
w	2.21	2.32	2.36	2.59	2.55	2.57
x	2.76	2.61	2.70	2.53	2.55	2.57
y	2.75	2.75	2.98	2.53	2.55	2.57
z	2.76	2.61	2.70	2.59	2.55	2.57

(Se-p and Cd-s, respectively) were also found for neutral Cd_6Se_6.[87]

In summary, all the NBA and the Mulliken charges and the HOMO-LUMO analysis of Iso-I lead to the conclusion of stable neutral Se_2 and positive Cd_2^+ subunits within the cluster. These species are only found in the cationic system, and this explains the special stability of the Iso-I structure.

D. $CdSe_2^+$ experimental and theoretical optical absorption spectra

The experimental absorption spectrum of the molecular $CdSe_2^+$ ions is compared to optical response calculations for both lowest energy structural candidates in Fig. 6. The experimental spectrum is dominated by two distinct absorption maxima at 2.17 eV (a) and 3.21 eV (b) and a broad absorption feature above 4 eV (c). Up to 4.19 eV, the experimental data points show a smooth absorption trend and the signal to noise ratio is very good so that the data points display almost no scattering around the 5-point adjacent average. One reason for the smooth trend is the effect of much more intense and stable laser irradiation generated by the new SFM extension. Beyond 4.19 eV, the experimental data are scattered much more around the 5-point adjacent average because this high energy region can only be accessed by the less intense and more fluctuating SHG of the signal wave. The oscillator strengths f of the TDDFT and EOM-CCSD calculations are convoluted with Gaussian functions, with a full width at half maximum of 0.33 eV, as a guide to the eye. All computed absorption spectra for Iso-I show two distinct absorption maxima and a more broad absorption feature around 4.25 eV. The EOM-CCSD calculation, however, clearly outperforms the other methods in terms of peak separation, even if peak **b** is slightly more blue-shifted. Both TDDFT calculations reveal very similar results. The EOM calculation (black line) is much closer to experiment for peak **a** but is more blue-shifted (as mentioned above) from the experiment and TDDFT calculations for peak **b**. The PBE0 transitions are somewhat higher in energy than

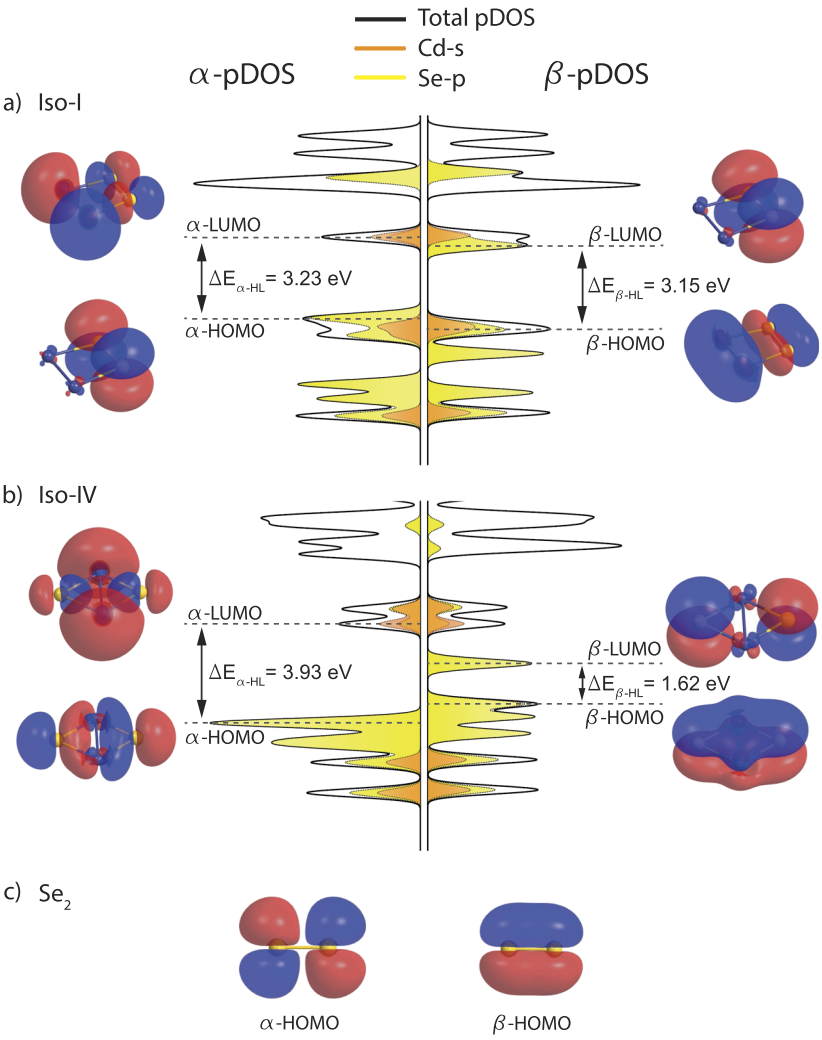

FIG. 5. α-pDOS and β-pDOS of $Cd_2Se_2^+$, with visualisation of the HOMO and LUMO and the HOMO-LUMO gaps for (a) Iso-I and (b) Iso-IV. (c) HOMO of neutral Se_2 (triplet state). The yellow area under the pDOS indicates the Se-p orbital contribution, whereas the orange area marks the Cd-s orbital contribution to the total pDOS (black line). All quantities are calculated at the PBE0/cc-pVTZ-PP level of theory.

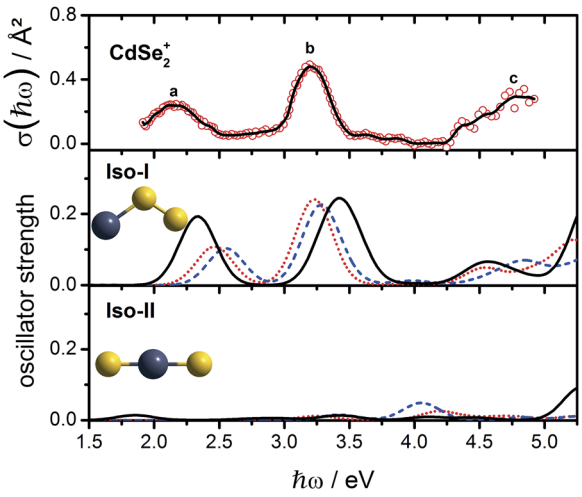

FIG. 6. Experimental $CdSe_2^+$ absorption cross section $\sigma(\hbar\omega)$ data points (red circles) and a 5-pt adjacent average as a guide to the eye (solid black line) compared to the optical absorption of Iso-I and Iso-II, calculated with EOM-CCSD (black line) and PBE0 (dashed blue line) as well as B3LYP (red dots) TDDFT calculations. The spectra are generated by Gaussian convolution of line spectra using a full width at half maximum of 0.33 eV.

the B3LYP results. For Iso-II, only low intensity optical transitions are obtained at all levels of theory, over the investigated energy range.

In Table VI, the oscillator strengths for the **a**, **b**, and **c** transitions are calculated. Table VI reveals that all computed oscillator strengths for Iso-I show a very good agreement with the experiment. The transition energies (denoted in round brackets) correspond to the maximum tuning points of the envelope Gaussian. The oscillator strengths for all transitions (**a**, **b**, and **c**) calculated with TDDFT tend to be smaller than those obtained by EOM-CCSD. Hence, the oscillator strengths calculated with TDDFT match the experimental data slightly better. By taking only the optical absorption spectra into account, no clear exclusion of Iso-II in the experiment is possible because the strong electronic transitions of Iso-I may mask a potential contribution of Iso-II. However, considering the large energy separation between these isomers, of more than 1.40 eV (see Fig. 2), the presence of Iso-II in the experiment is very unlikely. Taking all data into account, it can be assumed that the experimentally observable spectrum is solely caused by the presence of Iso-I.

TABLE VI. Oscillator strengths f of the experimentally observed transitions (**a**, **b**, and **c**) of $CdSe_2^+$ compared with the corresponding oscillator strengths of Iso-I from EOM-CCSD and TDDFT calculations. The experimental and Gaussian peak positions in eV of the corresponding level of theory are given in brackets. The experimentally observed oscillator strengths are calculated by Gaussian deconvolution according to $f = 0.911\ 03\ \text{Å}^{-2}(\text{eV})^{-1} \int_{Band} \sigma(\hbar\omega)d(\hbar\omega)$.[88]

Peak	f (Expt.)	f (EOMCCSD)	f (B3LYP)	f (PBE0)
a	0.116 (2.17)	0.190 (2.33)	0.108 (2.46)	0.103 (2.54)
b	0.186 (3.21)	0.280 (3.42)	0.240 (3.23)	0.237 (3.29)
c	0.196 (4.83)	0.108 (4.57)	0.112 (4.58)	0.135 (4.85)

In order to understand the nature of the optical transition, in Table VII we have conducted a Natural Transition Orbital (NTO) analysis of Iso-I for the transitions **a** and **b** at the PBE0/cc-pVTZ-PP level of theory, calculated with Chemissian.[85] An atomic shell Mulliken analysis of the NTOs was performed to obtain the contribution of the atomic basis functions to each NTO. Hence, we calculated, for each initial and final state NTO, the s/p/d basis set contributions from Cd and Se. For transitions **a** and **b**, the initial and final states correspond to a mixture of several states in the HOMO-LUMO region (HOMO-2, HOMO-1, HOMO, LUMO, LUMO+1, and LUMO+2). Moreover, the calculations also show a transition at 1.31 eV with 99% α-HOMO character in the initial state and 99% α-LUMO character in the final state, but with zero oscillator strength f. Thus, there is no pure HOMO-LUMO transition with $f > 0.00$. The NTOs corresponding to both transitions **a** and **b** show a dominant Se-p contribution. This is much more dominant than any Cd basis function. Regarding all s/p/d contributions to transition **a**, the Se-p percentage in the initial state is higher than in the final state, whereas the opposite is found for Cd-s and Cd-d. Hence, transition **a** comprises Se-p → Cd-s, Se-p → Se-p, and Se-p → Cd-d excitations. Taking all NTOs of transition **b** into account, no clear trend is discernible, but the same basis functions as for **a** (Cd-s, Cd-d and Se-p) contribute to the NTOs and again Se-p contributes most strongly to both the initial and final states. Both transitions, therefore, show strong Se-p character in the initial and final states.

E. $Cd_2Se_2^+$ experimental and theoretical optical absorption spectra

Figure 7 shows the experimental photodissociation spectrum of $Cd_2Se_2^+$. It displays two absorption maxima, a weaker one at 3.34 eV (**a**) and a more intense one around 4.68 eV (**b**). The analysis of all computed spectra show that the B3LYP and PBE0 data agree very well with the EOM-CCSD results concerning peak positions, intensities, and overall shape. In most cases, the optical absorption features calculated with B3LYP occur at slightly lower energies than those computed with PBE0 or EOM-CCSD. The experimental absorption

TABLE VII. Mulliken population analysis of the initial and final NTOs, which are responsible for the electronic transitions **a** and **b** of $CdSe_2^+$ (Iso-I) at the PBE0/cc-pVTZ-PP level of theory. The exact transition energies of the corresponding oscillator strengths are given in brackets. Only NTO pairs which contribute more than 10% to a specific electronic transition are shown [percentage p with $p(\text{NTO}) > 10\%$].

		Total s/p/d contributions			
		Initial orbitals		Final orbitals	
Transition	P (NTO)	Cd	Se	Cd	Se
a (2.50 eV)	46	20/0/0	0/80/0	22/0/23	0/55/0
	29	0/0/0	0/100/0	0/0/0	0/100/0
	26	1/0/0	0/99/0	6/0/0	0/94/0
b (3.28 eV)	54	0/0/0	0/100/0	0/0/0	0/100/0
	27	12/0/22	0/66/0	6/0/0	0/94/0
	19	23/0/0	0/77/0	21/0/19	0/60/0

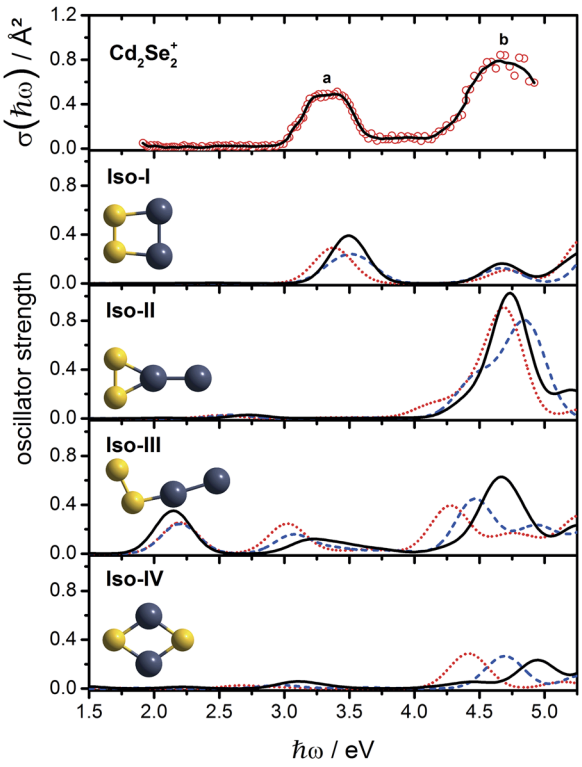

FIG. 7. Experimental $Cd_2Se_2^+$ absorption cross section $\sigma(\hbar\omega)$ data points (red circles) and a 5-pt adjacent average as a guide-to-the-eye (solid black line) compared to the optical absorption of Iso-I to Iso-IV calculated with PBE0 (dashed blue line) as well as B3LYP (red dots) TDDFT calculations and EOM-CCSD (black line) computations. The spectra are generated by Gaussian convolution of line spectra using a full width at half maximum of 0.33 eV.

energies of both maxima can be explained by the proposed GM (Iso-I). Regarding Iso-I at all levels of theory, it is evident that PBE0, B3LYP, and EOM-CCSD are in very good agreement with the experimental data. While the absorption spectra calculated with PBE0 and EOM-CCSD are somewhat more blue-shifted, the position of the optical absorption calculated with B3LYP matches almost perfectly with the experimental peak **a**. However for all calculations, the predicted relative peak intensities [$f(\mathbf{a}) > f(\mathbf{b})$] differ from the experimental observation [$\sigma(\mathbf{a}) < \sigma(\mathbf{b})$]. Taking into account the oscillator strengths of Iso-I listed in Table VIII, it is apparent that, in the case of peak **a**, the corresponding experimental oscillator strength is slightly smaller than the calculated ones. This observation agrees with the fact that the experimental cross sections here can be considered as lower limits on the total absorption cross sections. By contrast, the experimental oscillator strength of peak **b** clearly exceeds the calculated oscillator strength.

Based on the theoretically predicted structures and the calculated spectra, it is quite possible that at least two isomers contribute to the experimental spectrum. The "Y"-shape structure Iso-II shows a very strong absorption at the position of the maximum of peak **b** and a very weak broad absorption feature at 2.53 eV, which is not clearly observed in the experimental data. The optical spectra of Iso-III and Iso-IV are not consistent with the experimental data, as the broad absorption peaks of Iso-III and Iso-IV starting at 2.75 eV are not detected in the experimental spectrum and the first peak of Iso-III around 2.16 eV is also missing. Additionally, the fact that Iso-III is not a true minimum for calculations at the CCSD level and Iso-IV is significantly higher in energy than Iso-I [$\Delta E(\text{Iso-IV})_{\text{CCSD(T)}} = 0.33$ eV] makes the experimental presence of Iso-III and Iso-IV rather unlikely. Though the experimental absorption spectrum can be largely explained by Iso-I, the coexistence of Iso-II cannot be completely excluded experimentally.

In order to obtain a better understanding of the experimentally observed transitions **a** and **b**, Table IX shows the contributions of the s/p/d atomic basis functions to the initial and final NTO states for Iso-I. Interestingly, no d orbitals are involved in either of these transitions. In the case of Cd, only s-orbitals contribute to the initial states, whereas in the excited states, Cd-s and Cd-p orbitals are involved. In comparison to $CdSe_2^+$ (see Table VII), the percentage of Cd basis functions of $Cd_2Se_2^+$ is larger in both the initial and final states. Thus, the extent of the Cd contribution to the NTOs is increased by adding a second Cd atom to the system. Regarding Se in both cluster systems, only Se-p basis functions participate in the NTOs and these play a dominant role in the optical spectra of both $CdSe_2^+$ and $Cd_2Se_2^+$. Assuming that only valence electrons participate in the optical transitions, this is consistent with the dominant Se-p character in the HOMO and LUMO regions, as shown in Fig. 5. A more detailed analysis of Table IX helps to explain the nature of the

TABLE VIII. Oscillator strengths f of the experimentally observed transitions (**a** and **b**) of $Cd_2Se_2^+$ compared to the corresponding oscillator strengths of Iso-I from EOM-CCSD and TDDFT calculations. The * indicates the oscillator strengths of Iso-II regarding the transition **b**. The experimental and Gaussian peak positions in eV of the corresponding level of theory are given in brackets. The experimentally observed oscillator strengths are calculated by Gaussian deconvolution according to $f = 0.911\ 03\ \text{Å}^{-2}(\text{eV})^{-1} \int_{Band} \sigma(\hbar\omega)d(\hbar\omega)$.[88]

Peak	f (Expt.)	f (EOMCCSD)	f (B3LYP)	f (PBE0)
a	0.210 (3.34)	0.394 (3.50)	0.306 (3.38)	0.301 (3.52)
b	0.487 (4.69)	0.164 (4.69)	0.147 (4.71)	0.137 (4.69)
b*	0.487 (4.69)	1.710 (4.73)	1.183 (4.68)	1.236 (4.84)

TABLE IX. Mulliken analysis of the initial and final NTOs contributing to the electronic transitions **a** and **b** of $Cd_2Se_2^+$ (Iso-I) at the PBE0/cc-pVTZ-PP level of theory. The exact transition energies of the corresponding oscillator strengths are given in brackets. Only NTO pairs which contribute more than 10% to a specific transition are shown [p(NTO) >10%].

		Total s/p/d contributions			
		Initial orbitals		Final orbitals	
Transition	p(NTO)	Cd	Se	Cd	Se
a (3.40 eV)	35	57/0/0	0/43/0	23/29/0	0/48/0
	32	54/0/0	0/46/0	21/27/0	0/52/0
	26	0/0/0	0/100/0	0/0/0	0/100/0
a (3.59 eV)	51	27/0/0	0/73/0	23/30/0	0/47/0
	44	31/0/0	0/69/0	22/28/0	0/50/0
b (4.66 eV)	51	53/0/0	0/47/0	0/100/0	0/0/0
	48	49/0/0	0/51/0	0/100/0	0/0/0

electronic transitions. For transition **a**, the Se-p percentages in the initial and final states are roughly the same. However, the Cd contributions are quite different. Only Cd-s basis functions account for the initial NTO. This value is halved in the final state and is also mixed with Cd-p orbitals. For the next electronic transition at 3.59 eV, still belonging to absorption peak **a**, an increase of the Cd-p percentage with the simultaneous decrease of the Se-p contribution is observed. For this reason, the total electronic excitation exhibits a large proportion of Se-p → Cd-p character, which indicates charge-transfer during the electronic transition. The transition related to absorption peak **b** shows for the final state exclusive population of Cd-p orbitals and no contribution of Cd-p orbitals for the initial state. This excitation can clearly be attributed to the transitions Se-p → Cd-p and Cd-s → Cd-p. For transition **b**, again charge-transfer is observed from Se-p orbitals in the initial state to Cd-p orbitals in the final state. In summary, Se-p basis functions again play a crucial role in the relevant NTOs and Cd-p orbitals are very important for the final states. Furthermore, the electronic transitions exhibit significant charge-transfer character.

In general, the optical absorption spectra of larger CdSe nanoparticles show a first sharp transition, which is attributed to the HOMO-LUMO transition and is also known as the first excitonic feature.[89,90] The analysis of the optical excitation **a** of Iso-I exhibits large HOMO-LUMO contributions to the overall transition at 3.40 eV. The corresponding NTO with largest contribution is depicted in Fig. 10(a), which corresponds in its initial state to the α-HOMO-1 (cf. Fig. 5) and in its final state to the α-LUMO. The excitation from the β-HOMO to β-LUMO + 1 also contributes to this transition. It is striking that the two initial states α-HOMO-1 and β-HOMO, as well as the two final states α-LUMO and β-LUMO+1, have virtually the same shape. The DFT HOMO-LUMO gap $\Delta E_{\beta-\mathrm{HL}}$ = 3.15 eV is also close to the experimental absorption [E_{opt}(**a**) = 3.34 eV]. Hence, it is justified to mainly attribute the first absorption **a** to excitations of outer electrons in or near the HOMO-LUMO region.

The experimentally first observed transition **a** of $Cd_2Se_2^+$ shows a significant blue-shift in comparison to the first absorption peak of larger colloidal CdSe NPs or to the bandgap of bulk CdSe. For instance, the first absorption peak of $Cd_{33}Se_{33}$ and $Cd_{34}Se_{34}$ (particle diameter 1.5 nm) in toluene is located at 2.99 eV.[50] The first excitonic transition of larger CdSe NPs (particle diameter 2.1–6.4 nm) appears in the range 2.64–1.96 eV,[91] and the bulk CdSe bandgap is 1.7 eV, whereas transition **a** of $Cd_2Se_2^+$, at 3.34 eV, shows the strongest blue-shift. This is surprising since the experimentally discriminated structure of $Cd_2Se_2^+$ is Iso-I, which consists of a molecular Se_2 unit and thus differs very significantly from bulk CdSe or larger CdSe NPs in terms of bonding nature. Moreover, Iso-IV which is more similar to larger CdSe systems with respect to its structure and chemical (more ionic) bonding exhibits a first allowed transition at 0.59 eV at the PBE0/cc-pVTZ-PP level of theory, which is strongly red-shifted in comparison to the larger colloidal CdSe NPs and even to bulk CdSe. Hence, Iso-IV does not fit in with the trend of a stronger blue-shift of the absorption gap with smaller system size, which is predicted by the quantum confinement effect. However, differences between the compared systems must be considered, such as the reduced coordination number and charge state in the case of Iso-I and Iso-IV. Since the charge can also have a huge effect on the absorption gap, the optical properties of the small cationic, neutral, and anionic Cd_2Se_2 for Iso-I and Iso-IV are investigated in Sec. III F in more detail. A more thorough analysis of the predicted optical properties for Iso-IV is given at the end of Sec. III F.

F. Influence of charge *q* (=−1, 0, +1) on optical properties of $(Cd_2Se_2)^q$

In the following, the influence of the charge on the electronic excitations is studied for $(Cd_2Se_2)^q$ based on isomers Iso-I and Iso-IV, with calculated optical absorption spectra shown in Fig. 8 (Iso-I) and Fig. 9 (Iso-IV). The electronic excitations are calculated with TDDFT employing B3LYP/cc-pVTZ-PP (red dots) and PBE0/cc-pVTZ-PP (blue dashed line) for the first 60 excited states. As shown in Tables X and XI, all clusters except the anionic Iso-IV exhibit for the first transitions an oscillator strength of $f < 0.01$. Moreover the oscillator strengths of the first few transitions are in most cases zero or almost zero. This was also observed for larger Cd_nSe_m clusters, and the resulting states were characterized as dark excitonic states.[92] For all clusters studied here, the first few transitions exhibit very strong HOMO-LUMO character ($p \geq 95\%$, but with vanishing oscillator strengths). For both isomers, three maxima, which together display a characteristic absorption pattern, are labeled by **j**, **k**, and **h**. For Iso-I, **j** and **k** correspond to the absorption peaks **a** and **b** examined in Sec. III E. In each system, the comparison between the different charge states shows a clear trend regarding the **j**–**k**–**h** absorption pattern. The more the valence electrons are present in the system, the more red-shifted and the more intense are the optical absorptions.

In order to check whether the absorption maxima labeled by the same letter correspond to each other, the nature of the optical transition is investigated on the basis of absorption **j**

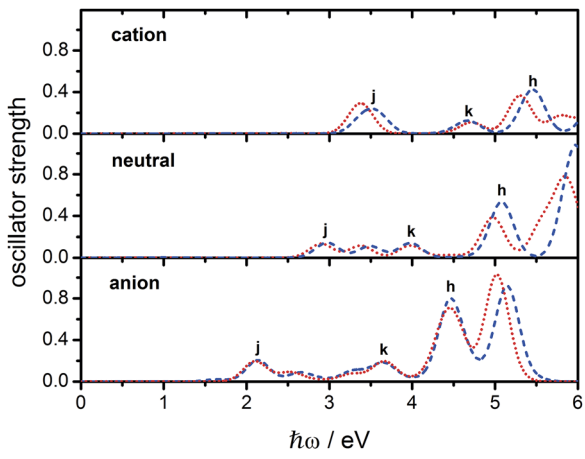

FIG. 8. Influence of the charge on the optical absorption spectra of Iso-I Cd_2Se_2. In TDDFT calculations, the hybrid PBE0 (blue dashed line) and B3LYP (red dots) functionals have been used. The spectra are generated by Gaussian convolution of line spectra using a full width at half maximum of 0.33 eV.

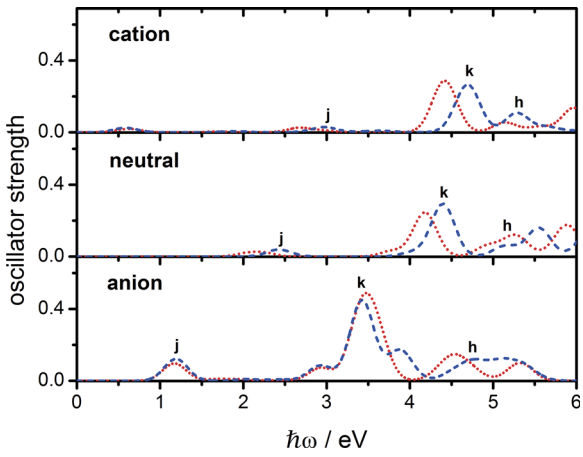

FIG. 9. Influence of the charge on the optical absorption spectra of Iso-IV Cd_2Se_2. In TDDFT calculations, the hybrid PBE0 (blue dashed line) and B3LYP (red dots) functionals have been used. The spectra are generated by Gaussian convolution of line spectra using a full width at half maximum of 0.33 eV.

for Iso-I. For this purpose, the NTO-pair with the largest contribution to transition **j** is visualized in Fig. 10. The NTOs are almost identical. The appropriate MO contributions correspond (for all charge states) to the HOMO-1 in the initial $|i\rangle$ and the LUMO in the final state $|f\rangle$. These observations lead to the conclusion that this transition, regardless of the molecular charge, has the same quantum chemical nature. For this reason, it is justified to speak of a red-shift of optical transition **j** with an increasing number of electrons in the system.

G. Comparison of $(Cd_2Se_2)^q$ (q = −1, 0, +1) with larger CdSe QDs

From a structural analysis of larger $(CdSe)_n$ NPs, Iso-IV seems to be a small geometrical building block since these NPs are built up of heteronuclear bonded hexagons and Iso-IV-like four-membered rings.[51–61] Hence, it seems surprising that the first allowed absorption peak **j** [E(**j**) = 2.38 eV] of neutral Iso-IV (which is the GM for neutral Cd_2Se_2) is red-shifted with respect to the first experimentally observed absorption peak of larger CdSe NPs: for example, $Cd_{33}Se_{33}$ and $Cd_{34}Se_{34}$ in toluene show the first absorption at E = 2.99 eV.[50] The same also applies for the first allowed electronic excitation of cationic and anionic Iso-IV.

As mentioned previously, for CdSe quantum dots, the blue-shift with decreasing particle size is due to the quantum confinement effect. This can be described using the effective mass approximation in terms of a quasi-particle in a three-dimensional box.[93] Hence, only the volume of the particle is taken into account as a geometric parameter. However, for very small systems consisting of only a few atoms, such as the Cd_2Se_2 cluster, a precise description has to consider the number of atoms and their spatial configuration explicitly with rigorous quantum chemical methods since optoelectronic properties are related to the geometry, as shown for $Cd_2Se_2^+$ in Fig. 7. Therefore, the simple particle in a three-dimensional box problem fails for very small CdSe clusters. For completeness, it should be mentioned that in recent studies, more advanced methods, such as Quantum Monte Carlo, DFT, TDDFT, and delta-self-consistent-field methods, have been applied to study the quantum confinement behavior of nanocrystals.[94–96]

At least three effects are responsible for the fact that the first transition of Iso-IV (whether neutral or charged) is not blue-shifted with respect to the optical absorption of larger CdSe NPs.[50,91]

TABLE XI. Transition energies and oscillator strengths for the first 8 excited states for Iso-IV for different total charges.

	Cation		Neutral		Anion	
No.	E/eV	f	E/eV	f	E/eV	f
1	0.40	0.00	1.70	0.00	1.19	0.12
2	0.59	0.02	2.38	0.02	1.83	0.00
3	1.10	0.00	2.46	0.00	1.85	0.00
4	1.90	0.01	2.48	0.02	2.04	0.01
5	2.21	0.00	2.77	0.00	2.15	0.00
6	2.32	0.00	2.97	0.00	2.42	0.01
7	2.44	0.00	3.11	0.00	2.45	0.00
8	2.67	0.00	4.04	0.02	2.55	0.00

TABLE X. Transition energies and oscillator strengths for the first 8 excited states for Iso-I for different total charges. The transition energy related to excitation **j** is shown in bold.

	Cation		Neutral		Anion	
No.	E/eV	f	E/eV	f	E/eV	f
1	1.74	0.00	0.95	0.00	0.88	0.00
2	1.75	0.00	2.75	0.00	1.63	0.02
3	1.75	0.00	2.81	0.00	1.83	0.00
4	2.07	0.00	2.90	0.00	2.09	0.00
5	2.15	0.00	**2.97**	0.14	**2.14**	0.19
6	2.53	0.00	3.27	0.00	2.18	0.00
7	**3.40**	0.14	3.49	0.11	2.28	0.00
8	3.41	0.00	3.97	0.10	2.39	0.00
8	3.41	0.00	3.97	0.10	2.39	0.00

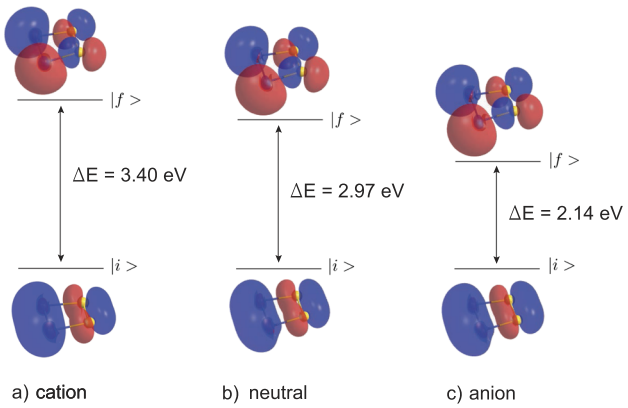

FIG. 10. Charge dependence of the optical properties, exemplified by the most intense electronic transition to the absorption band **j** for Iso-I. The NTOs with the largest percentage in this transition are shown.

(A) Special behavior of very small clusters:
The smallest bare semiconductor clusters do not obey the blue-shift of the optical absorption for increasingly smaller systems that one would expect from a particle in a box model. Nguyen *et al.* showed that in contradiction to the prediction of quantum confinement, the energy of the first electronic excitation E_{1st} (which is in most cases $f = 0.00$ for the Cd_nSe_m cluster) significantly increases from Cd_2Se_2 (E_{1st} = 1.70 eV) to Cd_3Se_3 (E_{1st} = 3.11 eV) by 1.41 eV.[97] In addition, Cd_4Se_4 (E_{1st} = 2.66 eV) and Cd_6Se_6 (E_{1st} = 2.80 eV) also exhibit larger absorption energies than Cd_2Se_2. The observed order of first transition energies $E_{1st}(Cd_3Se_3) > E_{1st}(Cd_6Se_6) > E_{1st}(Cd_4Se_4) > E_{1st}(Cd_2Se_2)$ clearly shows no simple dependence on system size. Even $Cd_{13}Se_{13}$ exhibits almost the same first transition energy as Cd_6Se_6.[98] The HOMO-LUMO gaps E_{HL} also show a similar behavior, and Cd_2Se_2 has significantly lower value ($E_{HL} \approx 1.1$ eV) than for larger Cd_nSe_n clusters ($E_{HL} > 1.5$ eV) at least up to $n = 16$.[59] In the series of small Cd_nS_n (n = 2–12) clusters, the smallest species Cd_2S_2 showed the smallest HOMO-LUMO gap, the smallest first optical transition, and the smallest first optical transition with non-zero oscillator strength.[99] This behavior was called a violation of the quantum confinement effect and was explained by the fact that such small clusters are rather low-dimensional surface-like particles, instead of three-dimensional (spherical) volume-like particles (such as larger NPs), and thus, they cannot be described by a simple three-dimensional particle in a box model. In Ref. 100, this non-quantum confinement behavior of small semiconductor clusters was attributed to the large effect of electron-electron interactions due to strong electron correlation effects in such very small systems. The violation of quantum confinement effects in small systems has also been confirmed for other semiconductor clusters such as ZnS and GaAs.[97,101] However, there are some systems, which seem to follow the confinement trend, even for very small sizes.[94,102] Hence, quantum effects, and the strong influence of the atomic arrangement on optoelectronic properties in very small semiconductor clusters, lead to the fact that simple confinement models (which are applicable to larger NPs) can no longer be used and more rigorous *ab initio* quantum chemical methods have to be employed.

(B) Effect of ligands:
In experiments, the quantum confinement effect is mostly studied for colloidal CdSe QDs.[17,91,100,103–105] Hence the impact of the surfactant ligands on the optoelectronic properties must be considered. This raises the question of how ligands influence the geometric and optoelectronic properties of the cluster. Puzder *et al.* investigated the geometries of bare and ligand passivated $(CdSe)_n$ (n = 5, 15, 33, 45) clusters and found the same structures for both cases.[106] The ligand passivation of clusters leads to the stabilisation of dangling bonds on the surface atoms (due to missing bonding partners).[107] Ligands with valence "lone pairs" of electrons act as electron donors and hence give rise to ligand-cluster charge transfer.[98] The ligands also tend to increase the HOMO-LUMO gap by stabilisation of the surface states (which typically lie within the bulk-like bandgap). The blue-shift of the HOMO by ligand passivation was investigated for $(CdSe)_n$ (n = 1–37).[60] CdSe clusters in the presence of ligands also display a blue-shift of the optical gap with respect to the bare clusters. Nguyen *et al.* investigated the effect of different numbers of water ligands on the optical transitions of the Cd_2Se_2 (Iso-IV) cluster.[97] They considered 2, 4, and 12 H_2O ligands and found a significantly large shift of the optical transitions and larger oscillator strengths with an increasing number of ligands. Whereas the first optical transition of bare Cd_2Se_2 is at 1.70 eV, the optical transition of Cd_2Se_2 with 12 water ligands is blue-shifted by more than 2.52 eV (moving to 4.22 eV). They found this trend for several $(CdSe)_n$ and $(ZnS)_n$ (n = 2, 3, 4, 6) clusters. Optical properties are not only influenced by the number of ligands coordinated to the cluster but also by the specific ligand type.[108,109] The ligand induced blue-shift of the optical absorption of small CdSe clusters was also reported for other ligand types such as phosphines,[109,110] amines,[109,111] pyridine,[109] phosphine oxides,[109] and thiols.[112]

The shape of the optical absorption spectrum is also strongly influenced by ligand passivation. This was shown by Stener *et al.* for the example of $Cd_{33}Se_{33}$.[107] At low energy, the optical absorption spectra of bare clusters have complicated shapes, with several small absorption intensities, whereas the optical absorption spectra of the ligand passivated clusters possess the same absorption signature as observed for CdSe QDs, i.e., the appearance of a very strong and sharp first absorption peak, which is typically associated with exciton phenomena. The analysis of the first transition causing the excitonic peak was attributed to the HOMO-LUMO transition with $p = 98\%$. In summary, the ligand passivation of CdSe clusters does not only lead to a huge blue-shift of the optical transitions but also to a significant change in the appearance of the absorption spectrum.

(C) Effect of solvent:
CdSe QDs and clusters in experiments are synthesized in solution, and hence, the effect of the solvent also has to be taken into account. The solvent also has a significant effect on the HOMO-LUMO gaps and on the optical absorption spectra.[109,111,113] It was found that the presence of the solvent causes a further blue-shift of the lowest energy electronic transition and this shift is more pronounced, the more polar the solvent. The extent of the solvent-induced blue-shift was found to be between 0.2 and 0.4 eV.[109,113]

In addition to the issues outlined above, there may also be discrepancies between theory and experiment regarding the optical properties of CdSe QDs or clusters, if either the level of theory is not appropriate (which may lead to an

under- or overestimation of the absorption gap) or if the experimental investigated CdSe QD sample is not monodisperse (comprising a range of particle sizes) and/or consists of more than one isomer. Characteristic absorption features may then not be visible, due to the overlap of different absorption profiles.

IV. CONCLUSIONS

In this joint experimental and theoretical study, the optical absorption spectra of bare $CdSe_2^+$ and $Cd_2Se_2^+$ clusters are analyzed. For both systems, the SFM region (3.04–4.19 eV) of the absorption spectra displays high quality of the experimental data, with a significantly enhanced signal to noise ratio. Both species show molecular-like optical absorption spectra, characterized by well-separated absorption peaks. In the case of $CdSe_2^+$, the experimental findings can be explained by the presence of Iso-I (a Se-unit with a Cd cation) only, while for $Cd_2Se_2^+$, the experimental data match our newly identified GM Iso-I (a trapezoid structure consisting of neutral Se_2 and charged Cd_2^+ dimers), whereas the absorption peak **b** can be explained by a coexistence of Iso-I and Iso-II ("Y"-shape structure). The investigated optical transitions indicate charge transfer from Se to Cd. The quantum chemical calculations, which correspond to the experimentally observed absorption peak of $CdSe_2^+$ and $Cd_2Se_2^+$, are a mixture of several transitions in the HOMO-LUMO region. Both clusters also exhibit lower lying electronic excitations with zero oscillator strengths, which can be attributed to almost pure HOMO-LUMO transitions. Additionally, the pDOS of $Cd_2Se_2^+$ shows for Iso-I and Iso-IV a dominant Se-p contribution to the HOMO and a significant Cd-s contribution to the LUMO, which is in accordance with larger CdSe NPs and to the valence and conduction band composition of bulk CdSe. The comparison of the first measured absorption peak of $Cd_2Se_2^+$ (located at 3.34 eV) to the optical gap of larger CdSe NPs and the CdSe bulk bandgap exhibits a significant blue-shift, although the $Cd_2Se_2^+$ GM isomer shows a completely different chemical bonding nature. By contrast, Iso-IV, the heteronuclear bonding isomer, which is also a small building-block of larger CdSe clusters, violates the expected quantum confinement trend. The main reasons for this are the special bonding nature of very small CdSe clusters and the absence of ligands and solvents.

Nevertheless, bare $Cd_2Se_2^+$ can be considered as a first step towards understanding the development of optical and electronic properties of CdSe NPs, starting from very small clusters. Moreover, it has been shown that for $Cd_2Se_2^+$, the charge has a significant influence on electronic, geometrical, and optical properties. In contrast to $Cd_2Se_2^+$, the neutral and anionic clusters do not form a stable neutral Se_2 unit, and therefore, the heteronuclear bonding structure Iso-IV is the highly preferred GM geometry. In summary, this combined experimental and theoretical study should be understood as a starting point for a better understanding of the evolution of the optoelectronic properties of CdSe clusters and nanosystems as a function of factors such as size, composition, charge state, and ligand effects.

SUPPLEMENTARY MATERIAL

In the supplementary material, we provide benchmark data for different basis sets and xc functionals for calculated optical properties of Cd_nSe_{m+}, making a direct comparison with the experimental data. This benchmark shows the best fit for PBE0/cc-pVTZ-PP and B3LYP/cc-pVTZ-PP. Furthermore we provide a detailed geometric analysis of the bond length dependency on the charge for Iso-I and Iso-IV of Cd_2Se_{2+}.

ACKNOWLEDGMENTS

We thank Jorge A. Vargas (UNAM, Mexico) for sharing the MEGA code. We acknowledge financial support from the Deutsche Forschungsgemeinschaft (Grant No. SCHA 885/15-1) and COST action MP0903 (NANOALLOYS). M.J. acknowledges a scholarship of the Mercksche Gesellschaft für Kunst und Wissenschaft. A.S. acknowledges funding by the Austrian Science Fund (FWF) within the Lise-Meitner fellowship (M 2364). The calculations were performed on the following HPC facilities: The University of Birmingham BlueBEAR facility (see http://www.bear.bham.ac.uk/bluebear for more details) and Thomas, the UK National Tier 2 High Performance Computing Hub in Materials and Molecular Modelling, which was partially funded by EPSRC (No. EP/P020194), via our membership of the UK's HEC Materials Chemistry Consortium funded by EPSRC (No. EP/L000202).

[1] J. Borbinha, IEEE Solid-State Circuits Mag. **5**(1), 40 (2013).
[2] D. E. Root, IEEE Microwave Mag. **13**, 45 (2012).
[3] M. M. Waldrop, Nature **530**, 144 (2016).
[4] T. J. K. Liu, U. Sikder, K. Kato, and V. Stojanovic, in *Procedings of the IEEE International Conference on Micro Electro Mechanical Systems (MEMS)* (IEEE, 2017), p. 1.
[5] B. Ullmann and T. Grasser, E I Elektr. Inf. **134**, 349 (2017).
[6] Y. Shen, N. C. Harris, D. Englund, and M. Soljačić, Nat. Photonics **11**, 441 (2017); e-print arXiv:1610.02365.
[7] G. P. C. Drummen, Int. J. Mol. Sci. **11**, 154 (2010).
[8] M. Saad, N. Samsi, O. Hassan, M. Yahya, M. Mohamad Taib, A. Ali, and R. Zakaria, MATEC Web Conf. **154**, 01039 (2018).
[9] J. Chen, V. Hardev, and J. Yurek, Inf. Disp. **29**(1), 12 (2013).
[10] F. Zhang, S. Wang, L. Wang, Q. Lin, H. Shen, W. Cao, C. Yang, H. Wang, L. Yu, Z. Du, J. Xue, and L. S. Li, Nanoscale **8**, 12182 (2016).
[11] X. Gao, Y. Cui, R. M. Levenson, L. W. K. Chung, and S. Nie, Nat. Biotechnol. **22**, 969 (2004).
[12] M. J. Bowers II, J. R. Mcbride, and S. J. Rosenthal, J. Am. Chem. Soc. **127**, 15378 (2005).
[13] V. I. Klimov, Science **290**, 314 (2000).
[14] R. Gross and A. Marx, *Festkörperphysik*, 1st ed. (Oldenburg Verlag München, München, 2010).
[15] M. Grundmann, *The Physics of Semiconductors an Introduction Including Nanophysics and Applications*, 3rd ed. (Springer, Berlin, 2010).
[16] C. Kittel, *Introduction to Solid State Physics*, 8th ed. (John Wiley Sons, Inc., New York, 2004); e-print arXiv:1011.1669v3.
[17] C. B. Murray, D. J. Norris, and M. G. Bawendi, J. Am. Chem. Soc. **115**, 8706 (1993).
[18] M. Makkar and R. Viswanatha, RSC Adv. **8**, 22103 (2018).
[19] Y. Shirasaki, G. J. Supran, M. G. Bawendi, and V. Bulović, Nat. Photonics **7**, 13 (2013).
[20] M. G. Bawendi, A. R. Kortan, M. L. Steigerwald, and L. E. Brus, J. Chem. Phys. **91**, 7282 (1989).
[21] M. Bawendi, W. Wilson, L. Rothberg, P. Carroll, T. Jedju, M. Steigerwald, and L. Brus, Phys. Rev. Lett. **65**, 1623 (1990).
[22] M. Bawendi, Annu. Rev. Phys. Chem. **41**, 477 (1990).
[23] L. Brus, Appl. Phys. A Solids Surfaces **53**, 465 (1991).
[24] A. Aboulfotouh, B. M. Fikry, M. Mohamed, M. Omar, H. Rady, and Y. Elbashar, Opt. Quantum Electron. **50**, 115 (2018).

[25]Y. Wang, Y. Zhang, F. Wang, D. E. Giblin, J. Hoy, H. W. Rohrs, R. A. Loomis, and W. E. Buhro, Chem. Mater. **26**, 2233 (2014).
[26]B. M. Cossairt, P. Juhas, S. Billinge, and J. S. Owen, J. Phys. Chem. Lett. **2**, 3075 (2011).
[27]C. de Mello Donegá and R. Koole, J. Phys. Chem. C **113**, 6511 (2009).
[28]J. Jasieniak and P. Mulvaney, J. Am. Chem. Soc. **129**, 2841 (2007).
[29]V. Biju, Y. Makita, A. Sonoda, H. Yokoyama, Y. Baba, and M. Ishikawa, J. Phys. Chem. B **109**, 13899 (2005).
[30]Z. Deng, L. Cao, F. Tang, and B. Zou, J. Phys. Chem. B **109**, 16671 (2005).
[31]C. Leatherdale and W. Woo, J. Phys. Chem. B **106**, 7619 (2002).
[32]V. N. Soloviev, A. Eichhöfer, D. Fenske, and U. Banin, J. Am. Chem. Soc. **123**, 2354 (2001).
[33]V. N. Soloviev, A. Eichhöfer, D. Fenske, and U. Banin, Phys. Status Solidi B **224**, 285 (2001).
[34]L. H. Qu, Z. A. Peng, and X. G. Peng, Nano Lett. **1**, 333 (2001).
[35]D. Norris and M. Bawendi, Phys. Rev. B **53**, 16338 (1996).
[36]F. S. Riehle, R. Bienert, R. Thomann, G. a. Urban, and M. Krüger, Nano Lett. **9**, 514 (2009).
[37]K. J. Nordell, E. M. Boatman, and G. C. Lisensky, J. Chem. Educ. **82**, 1697 (2005).
[38]B. O. Dabbousi, J. Rodriguez, F. V. Mikulec, J. R. Heine, H. Mattoussi, R. Ober, K. F. Jensen, and M. G. Bawendi, J. Phys. Chem. B **101**, 9463 (1997).
[39]B. Zorman, M. V. Ramakrishna, and R. A. Friesner, J. Phys. Chem. **99**, 7649 (1995).
[40]C. Delerue, G. Allan, and M. Lannoo, J. Lumin. **80**, 65 (1998).
[41]V. Albe, C. Jouanin, and D. Bertho, Phys. Rev. B **58**, 4713 (1998).
[42]S. Reimann and M. Manninen, Rev. Mod. Phys. **74**, 1283 (2002).
[43]A. P. Alivisatos, Science **271**, 933 (1996).
[44]A. P. Alivisatos, J. Phys. Chem. **100**, 13226 (1996).
[45]D. M. Wood and N. W. Ashcroft, Phys. Rev. B **25**, 6255 (1982).
[46]Y. Wang and N. Herron, J. Phys. Chem. **95**, 525 (1991).
[47]A. M. Smith and S. Nie, Acc. Chem. Res. **43**, 190 (2010).
[48]T. Orii, S. Kaito, K. Matsuishi, S. Onari, and T. Arai, J. Phys. Condens. Matter **9**, 4483 (1999).
[49]H. Zhang, X. Peng, L. Sun, and F. Liu, MATEC Web Conf. **26**, 1006 (2015).
[50]A. Kasuya, R. Sivamohan, Y. A. Barnakov, I. M. Dmitruk, T. Nirasawa, V. R. Romanyuk, V. Kumar, S. V. Mamykin, K. Tohji, B. Jeyadevan, K. Shinoda, T. Kudo, O. Terasaki, Z. Liu, R. V. Belosludov, V. Sundararajan, and Y. Kawazoe, Nat. Mater. **3**, 99 (2004).
[51]M. M. Sigalas, E. N. Koukaras, and A. D. Zdetsis, RSC Adv. **4**, 14613 (2014).
[52]M. Troparevsky, L. Kronik, and J. Chelikowsky, Phys. Rev. B **65**, 033311 (2001).
[53]M. C. Troparevsky and J. R. Chelikowsky, J. Chem. Phys. **114**, 943 (2001).
[54]P. Deglmann, R. Ahlrichs, and K. Tsereteli, J. Chem. Phys. **116**, 1585 (2002).
[55]J. M. Matxain, J. M. Mercero, J. E. Fowler, and J. M. Ugalde, J. Phys. Chem. A **108**, 10502 (2004).
[56]A. Puzder, A. J. Williamson, N. Zaitseva, G. Galli, L. Manna, and A. P. Alivisatos, Nano Lett. **4**, 2361 (2004).
[57]S. Botti and M. A. Marques, Phys. Rev. B **75**, 035311 (2007); e-print arXiv:0605517 [cond-mat].
[58]M. Lopez Del Puerto, M. L. Tiago, and J. R. Chelikowsky, Phys. Rev. B **77**, 045404 (2008).
[59]P. Chandra, P. Seal, S. Sen, H. Ågren, and S. Chakrabarti, Comput. Mater. Sci. **44**, 728 (2008).
[60]K. A. Nguyen, P. N. Day, and R. Pachter, J. Phys. Chem. **114**, 16197 (2010).
[61]L. G. Gutsev, N. S. Dalal, and G. L. Gutsev, J. Phys. Chem. C **119**, 6261 (2015).
[62]E. Sanville, A. Burnin, and J. J. BelBruno, J. Phys. Chem. A **110**, 2378 (2006).
[63]A. Shayeghi, R. L. Johnston, and R. Schäfer, Phys. Chem. Chem. Phys. **15**, 19715 (2013).
[64]A. Shayeghi, D. A. Götz, R. L. Johnston, and R. Schäfer, Eur. Phys. J. D **69**, 152 (2015).
[65]A. Shayeghi, C. J. Heard, R. L. Johnston, and R. Schäfer, J. Chem. Phys. **140**, 054312 (2014).
[66]A. Shayeghi, L. F. Pašteka, D. A. Götz, P. Schwerdtfeger, and R. Schäfer, Phys. Chem. Chem. Phys. **20**, 9108 (2018).
[67]A. Shayeghi, R. L. Johnston, and R. Schäfer, J. Chem. Phys. **141**, 181104 (2014).
[68]J. A. Vargas, F. Buendía, and M. R. Beltrán, J. Phys. Chem. C **121**, 10982 (2017).
[69]A. Shayeghi, D. Götz, J. B. A. Davis, R. Schäfer, and R. L. Johnston, Phys. Chem. Chem. Phys. **17**, 2104 (2015).
[70]J. B. Davis, A. Shayeghi, S. L. Horswell, and R. L. Johnston, Nanoscale **7**, 14032 (2015).
[71]G. Kresse and J. Furthmüller, Phys. Rev. B **54**, 11169 (1996).
[72]G. Kresse and J. Hafner, Phys. Rev. B **49**, 14251 (1994).
[73]G. Kresse and J. Hafner, Phys. Rev. B **47**, 558 (1993).
[74]G. Kresse and J. Furthmüller, Comput. Mater. Sci. **6**, 15 (1996).
[75]J. P. Perdew, K. Burke, and M. Ernzerhof, Phys. Rev. Lett. **77**, 3865 (1996).
[76]G. Kresse and D. Joubert, Phys. Rev. B **59**, 1758 (1999).
[77]M. Valiev, E. J. Bylaska, N. Govind, K. Kowalski, T. P. Straatsma, H. J. J. V. Dam, D. Wang, J. Nieplocha, E. Apra, T. L. Windus, and W. A. D. Jong, Comput. Phys. Commun. **181**, 1477 (2010).
[78]C. Adamo and V. Barone, J. Chem. Phys. **110**, 6158 (1999); e-print arXiv:1011.1669v3.
[79]A. D. Becke, J. Chem. Phys. **98**, 5648 (1993); e-print arXiv:z0024.
[80]K. A. Peterson, J. Chem. Phys. **119**, 11099 (2003).
[81]D. Figgen, G. Rauhut, M. Dolg, and H. Stoll, Chem. Phys. **311**, 227 (2005).
[82]K. A. Peterson and C. Puzzarini, Theor. Chem. Acc. **114**, 283 (2005).
[83]M. J. Frisch, G. W. Trucks, H. B. Schlegel, G. E. Scuseria, M. A. Robb, J. R. Cheeseman, G. Scalmani, B. Barone, B. Mennucci, G. A. Petersson, H. Nakatsuji, M. Caricato, X. Li, H. Hratchian, A. F. Izmaylov, J. Bloino, G. Zheng, J. L. Sonnenberg, M. Hada, M. Ehara, K. Toyota, R. Fukuda, J. Hasegawa, M. Ishida, T. Nakajima, Y. Honda, O. Kitao, H. Nakai, T. Vreven, J. J. Montgomery, J. E. Peralta, F. Ogliaro, M. Bearpark, J. J. Heyd, E. Brothers, V. Kudin, V. N. Staroverov, R. Kobayashi, J. Normand, K. Raghavachari, A. Rendell, J. C. Burant, S. S. Iyengar, J. Tomasi, M. Cossi, N. Rega, J. M. Millam, M. Klene, J. E. Knox, J. B. Cross, V. Bakken, C. Adamo, J. Jaramillo, R. Gomperts, R. E. Stratmann, O. Yazyev, A. J. Austin, R. Cammi, C. Pomelli, J. W. Ochterski, R. Martin, K. Norokuma, V. G. Zakrzewski, G. A. Voth, P. Salvador, J. J. Dannenberg, S. Dapprich, A. D. Daniels, Ö. Farkas, J. B. Forseman, J. V. Ortiz, J. Cioslowski, and D. J. Fox, GAUSSIAN 09, Revision D.01, Gaussian, Inc., Wallingford, CT, 2009.
[84]P. Yang, S. Tretiak, A. E. Masunov, and S. Ivanov, J. Chem. Phys. **129**, 074709 (2008).
[85]L. Skripnikov, "Chemissian, A computer program to analyse and visualise quantum-chemical calculations" (2017), https://www.chemissian.com/.
[86]N. Chestnoy, R. Hull, and L. E. Brus, J. Chem. Phys. **85**, 2237 (1986).
[87]P. Ganesan and S. Lakshmipathi, Physica E **83**, 284 (2016).
[88]J. Friedrich, S. Gilb, O. T. Ehrler, A. Behrendt, and M. M. Kappes, J. Chem. Phys. **117**, 2635 (2002).
[89]V. Ptatschek, T. Schmidt, M. Lerch, G. Müller, L. Spanhel, A. Emmerling, J. Fricke, A. Foitzik, and E. Langer, Ber. Bunsenges. Phys. Chem. **102**, 85 (1998).
[90]A. P. Alivisatos, A. L. Harris, N. J. Levinos, M. L. Steigerwald, and L. E. Brus, J. Chem. Phys. **89**, 4001 (1988).
[91]J. Jasieniak, M. Califano, and S. E. Watkins, ACS Nano **5**, 5888 (2011).
[92]M. L. Del Puerto, M. L. Tiago, and J. R. Chelikowsky, Phys. Rev. Lett. **97**, 096401 (2006); e-print arXiv:0608521 [cond-mat].
[93]S. V. Gaponenko, *Optical Properties of Semiconductor Nanocrystals* (Cambridge University Press, Cambridge, 1998).
[94]H. C. Weissker, J. Furthmüller, and F. Bechstedt, Phys. Rev. B **69**, 115310 (2004).
[95]N. D. Drummond, A. J. Williamson, R. J. Needs, and G. Galli, Phys. Rev. Lett. **95**, 096801 (2005); e-print arXiv:0801.0381v1.
[96]J. Y. Raty, G. Galli, C. Bostedt, T. W. van Buuren, and L. J. Terminello, Phys. Rev. Lett. **90**, 037401 (2003).
[97]K. A. Nguyen, R. Pachter, and P. N. Day, J. Chem. Theory Comput. **9**, 3581 (2013).
[98]R. Nadler and J. F. Sanz, Theor. Chem. Acc. **132**, 1342 (2013).
[99]G. L. Gutsev, R. H. O'Neal, K. G. Belay, and C. A. Weatherford, Chem. Phys. **368**, 113 (2010).
[100]V. Proshchenko and Y. Dahnovsky, Phys. Chem. Chem. Phys. **16**, 7555 (2014).
[101]P. Karamanis, C. Pouchan, C. A. Weatherford, and G. L. Gutsev, J. Phys. Chem. C **115**, 97 (2011).
[102]A. J. Williamson, J. C. Grossman, R. Q. Hood, A. Puzder, and G. Galli, Phys. Rev. Lett. **89**, 196803 (2002).

[103]S. Kudera, M. Zanella, C. Giannini, A. Rizzo, Y. Li, G. Gigli, R. Cingolani, G. Ciccarella, W. Spahl, W. J. Parak, and L. Manna, Adv. Mater. **19**, 548 (2007).
[104]J. Jasieniak, L. Smith, J. van Embden, P. Mulvaney, and M. Califano, J. Phys. Chem. C **113**, 19468 (2009).
[105]W. W. Yu, L. Qu, W. Guo, and X. Peng, Chem. Mater. **15**, 2854 (2003).
[106]A. Puzder, A. J. Williamson, F. Gygi, and G. Galli, Phys. Rev. Lett. **92**, 217401 (2004).
[107]M. Del Ben, R. W. A. Havenith, R. Broer, and M. Stener, J. Phys. Chem. C **115**, 16782 (2011).
[108]B. P. Bloom, L. B. Zhao, Y. Wang, D. H. Waldeck, R. Liu, P. Zhang, and D. N. Beratan, J. Phys. Chem. C **117**, 22401 (2013).
[109]S. A. Fischer, A. M. Crotty, S. V. Kilina, S. A. Ivanov, and S. Tretiak, Nanoscale **4**, 904 (2012).
[110]S.-P. Yu, D.-L. Huang, Z.-G. Zhao, M.-L. Yang, and M.-H. Yang, J. Cluster Sci. **28**, 1825 (2017).
[111]J. M. Azpiroz, J. M. Matxain, I. Infante, X. Lopez, and J. M. Ugalde, Phys. Chem. Chem. Phys. **15**, 10996 (2013).
[112]S. Xu, C. Wang, and Y. Cui, J. Mol. Model. **16**, 469 (2010).
[113]V. V. Albert, S. A. Ivanov, S. Tretiak, and S. V. Kilina, J. Phys. Chem. C **115**, 15793 (2011).